Transition Met Chem (2011) 36:387–393
DOI 10.1007/s11243-011-9481-3

Catalytic partial oxidation of methanol over Au–Pd bimetallic catalysts: a comparative study of SBA-16, SBA-16-CeO_2, and CeO_2 as supports

Li Chen · Shuhua Wang · Chao Chen · Ning Zhang

Received: 29 January 2011 / Accepted: 9 March 2011 / Published online: 2 April 2011

Abstract Au–Pd catalysts supported on SBA-16, SBA-16-CeO_2, and CeO_2 had been studied for partial oxidation of methanol to produce H_2. The physicochemical characteristics of the catalysts prepared by deposition–precipitation using urea hydrolysis were examined by inductively coupled plasma atomic emission spectroscopy (ICP-AES), Brunauer-Emmett-Teller (BET), X-ray powder diffraction (XRD), Temperature-programmed reduction (TPR), and H_2 temperature-programmed desorption (H_2-TPD) analyses. The results show that Au_xPd_y alloys are observed in Au–Pd/SBA-16 and Au–Pd/SBA-16-CeO_2 catalysts. The catalytic results demonstrate that both Au–Pd/SBA-16 and Au–Pd/SBA-16-CeO_2 catalysts exhibit higher activity and lower CO selectivity than the Au–Pd/CeO_2 catalyst. This could be ascribed to the formation of Au_xPd_y alloys. The comparison of the Au–Pd/SBA-16 and Au–Pd/SBA-16-CeO_2 catalysts reveals that the Au–Pd/SBA-16-CeO_2 shows the lower CO selectivity, probably due to the presence of CeO_2.

Introduction

The polymer electrolyte fuel cell (PEMFC) using hydrogen is the most promising fuel cell for solving some of the serious energy-related problems [1, 2]. In order to avoid the technical difficulties of transportation, storage, and distribution of hydrogen, the fuel can be generated in an on-board steam reformer, which produces hydrogen from liquid fuels. Methanol is regarded as a primary candidate because of its abundance, high hydrogen to carbon (H/C) atomic ratio, and safe storage [3]. There are several reaction pathways for on-site hydrogen production from methanol, such as methanol decomposition (MD) [4], steam reforming of methanol (SRM) [5, 6], partial oxidation of methanol (POM) [7, 8], and oxidative steam reforming of methanol (OSRM) [9, 10]. Among them, POM is considered to be a suitable method due to its exothermic reaction, rapid reaction rate and using air or oxygen as oxidant instead of steam.

Supported Pd has been extensively utilized as a catalyst for H_2 generation from methanol by POM [11]. However, the main disadvantage of these catalysts is the formation of considerable amounts of CO, which is a known poisonous component for the PEMFC anode. Recently, numerous attempts have been made to modify the catalytic performances of Pd catalysts by the addition of Au, Cu, Zn, and so on [12–14]. Among these additives, Au has attracted great attention, due to its excellent catalytic activity for CO oxidation at low temperature [15, 16]. Up to now, many Au–Pd systems have revealed the synergistic effect of Au and Pd leading to the formation of Au_xPd_y alloys, which were favorable to the improvement of the activity and selectivity for the POM reaction [12].

To obtain effective Au_xPd_y alloy catalysts for the POM reaction, the supports play a key role because of their surface areas and the interactions between the metals and supports, which affect the formation of Au_xPd_y alloys. Mesoporous silica, as a kind of support material, has recently been of great interest, because of its large surface area, high thermal stability, and well-ordered structure, which promotes the formation and dispersion of bimetallic alloys [14]. Based on the above-mentioned previous work,

L. Chen · S. Wang (✉) · C. Chen · N. Zhang (✉)
Department of Chemistry, Nanchang University, Nanchang 330031, People's Republic of China
e-mail: shwang@ncu.edu.cn

N. Zhang
e-mail: nzhang.ncu@163.com

we focused on SBA-16 supports, which possess high surface area and 3-D cubic arrangement of cage-like mesopores [17–20]. Compared to the unidirectional pore mesoporous materials, SBA-16 could be more favorable for the reactants to access the catalytic sites, and the diffusion of products, owing to the unique 3-D channel network [17]. Additionally, we also noticed that CeO_2 was a very active support for the further oxidation of CO into CO_2, because it has high oxygen storage capacity and oxygen vacancies in the fluorite oxide structure [21–23]. Therefore, in this study, we prepared Au–Pd/SBA-16, Au–Pd/SBA-16-CeO_2, and Au–Pd/CeO_2 catalysts by deposition–precipitation technique using urea as precipitating agent. The activities for H_2 production from POM reaction on these catalysts were investigated. Scanning electron micrographs (SEM), ICP-AES, XRD, BET, TPR, and H_2-TPD analyses were used to identify the characteristics of these supports and catalysts. To the best of our knowledge, it is the first time that SBA-16 was utilized as a support for the POM reaction.

Experimental

Triblock copolymer Pluronic F127 was purchased from Aldrich. Other chemicals were obtained from Sinopharm Chemical Reagent co. All chemicals were analytical reagents. Deionized water was used for the catalyst preparation.

Support preparation

The mesoporous SBA-16 material was synthesized under acidic conditions, using Triblock copolymer Pluronic F127 as a structure-directing agent and TEOS as the silica source [24]. F127 (1.2 g) was added to HCl (1.75 mol/L, 60 g) aqueous solution and allowed to stir at 30 °C overnight, and then TEOS (4.0 mL) was added to this solution under vigorous magnetic stirring. After 10-min stirring, the mixture was kept under static conditions at 30 °C for 20 h. Finally, the solid products were collected by filtration, washed with ethanol, dried, and calcined at 550 °C with a heating rate of 2 °C/min in air for 5 h in order to remove the organic template.

CeO_2 support was prepared by precipitation method. The appropriate quantities of $(NH_4)_2Ce(NO_3)_6$ (0.1 mol/L) were dissolved in deionized water with constant stirring. Into this solution, polyethylene glycol (PEG-4000) as protection agent was added. Then, $NH_3{\cdot}H_2O$ (5 vol.%) was slowly added to it until completely precipitated. The mixture was refluxed at 70 °C for 4 h, filtered, and the solid washed with ethanol thoroughly. The sample was dried at 70 °C overnight and calcined at 500 °C for 4 h. The binary support, SBA-16-CeO_2, with a mass ratio of 5:5 was prepared in much the same way as CeO_2 support except that a certain amount of SBA-16 was added to the $(NH_4)_2Ce(NO_3)_6$ (0.1 mol/L) solution.

Catalyst preparation

The Au–Pd/SBA-16, Au–Pd/SBA-16-CeO_2, and Au–Pd/CeO_2 catalysts were prepared by deposition–precipitation with urea method. The appropriate quantities of $HAuCl_4$ (5.08 mL 0.01 mol/L) and $PdCl_2$ (9.40 mL 0.01 mol/L) were dissolved in 100 mL deionized water containing the urea. After adding supports (1.0 g) to the solution (initial pH $\approx$ 2), the suspension was vigorously stirred at 80 °C for 8 h (pH increases), and then the solvents were removed by rotary evaporator. Afterward, the solids were washed several times to eliminate Cl^-. Finally, the obtained samples were oven dried at 60 °C for 24 h and calcined at 400 °C for 2 h. The results of ICP-AES indicated that total load of the deposit noble metals was 2.0 wt% (Au: Pd = 5:5 wt/wt).

Characterization of samples

The composition of the catalysts was measured by ICP-AES using an American PE Corporation's Optima 5300 DV. The textural characteristics of the supports and catalysts were analyzed by N_2 physisorption method. N_2 adsorption and desorption isotherms were performed at −196 °C on a Micromeritics ASAP2020C instrument. The samples were outgassed in vacuum ($\approx$1 μm Hg) at 300 °C for 10 h before the measurement. The pore diameter was calculated from the analysis of desorption branch of the isotherm by the BJH (Barrett-Joyner-Halenda) method. XRD patterns were recorded on a Bruker AXS D8Focus diffractometer operating at 40 kV and 30 mA with Cu target Kα-ray irradiation. Diffraction data were collected between 0.5° and 10° with a step size of 0.01° and a step time of 2 s and 20°–70° with a scanning rate of 1°/min. The SEM was taken on a FEI SIRION electron microscope with an acceleration voltage of 5 kV. The sample was deposited on a sample holder with an adhesive carbon foil and sputtered with gold prior to imaging.

TPR experiments were carried out on a Chemisorb 2750 instrument over 0.1 g catalyst. The samples were heated from room temperature to 300 °C under flowing high-purity argon (50 mL/min) at a rate of 10 °C/min for 1 h in order to remove possible impurities. After cooling to room temperature, a reducing gas composed of 10% H_2/Ar was employed at a flow rate of 50 mL/min, with a heating ramp of 10 °C/min. The H_2 consumption was determined by gas chromatography equipped with a thermal conductivity detector.

H_2-TPD was carried out on an in-house apparatus. Prior to the TPD experiment, 0.1 g of the samples was reduced at 350 °C for 2 h using a flow of high-purity H_2 (30 mL/min) and then cooling to room temperature in argon (40 mL/min). H_2 was pulsed until adsorption was saturated. Finally, the samples were heated to 400 °C at a rate of 10 °C/min to record the H_2-TPD curves.

Catalytic activity measurements

Partial oxidation of methanol was carried out at atmospheric pressure in a continuous micro-reactor, which was placed inside a programmable furnace. The catalyst (0.1 g) was reduced in situ first in H_2 flow (30 mL/min) at 350 °C for 2 h and then cooled to the reaction temperature. Methanol was fed into the pre-heater by means of a Lab-Alliance liquid pump (Model: Series II-240). The oxygen and nitrogen (balanced) flows were adjusted by a mass flow controller. The molar ratio of O_2/CH_3OH was kept at 0.3, and the reaction was performed from 200 to 450 °C. The compositions were analyzed using an on-line gas chromatograph with a thermal conductor detector. A Porapak Q column was used to separate CH_3OH, H_2O, and CO_2, and a 5Å molecular sieve column was employed to separate H_2 and CO. The CH_3OH conversion, O_2 conversion, H_2 selectivity, and CO selectivity were defined as below:

$$\text{CH}_3\text{OH conversion } (\%) = \left(\frac{\text{moles of CH}_3\text{OH consumed}}{\text{moles of CH}_3\text{OH fed}}\right) \times 100\%$$

$$\text{O}_2\text{ conversion } (\%) = \left(\frac{\text{moles of O}_2\text{ consumed}}{\text{moles of O}_2\text{ fed}}\right) \times 100\%$$

$$\text{H}_2\text{ selectivity } (\%) = \left(\frac{\text{moles of H}_2\text{ produced} \times 0.5}{\text{moles of CH}_3\text{OH consumed}}\right) \times 100\%$$

$$\text{CO selectivity } (\%) = \left(\frac{\text{moles of CO produced}}{\text{moles of CH}_3\text{OH consumed}}\right) \times 100\%$$

Results and discussion

Characterization of mesoporous SBA-16 support

Figure 1A shows the small-angle XRD pattern of calcined SBA-16. A pattern with three well-resolved peaks is observed at 2θ value of 0.88°, 1.36°, and 1.70° that matched well with the reported (110), (200), and (211) plane reflections of cubic mesoporous structure [25]. The d-spacing of (110) plane calculated from Bragg's law is approximately 97 Å, which is also in the mesoporous range. The N_2 adsorption–desorption isotherm and pore size distribution of SBA-16 are presented in Fig. 1B and Table 1. As shown in Fig. 1B, the adsorbent exhibits reversible type-IV behavior with a typical H2 hysteresis loop and a narrow pore size distribution, indicating that the mesopores have uniform cage-like pore structure. As listed in Table 1, the synthesized SBA-16 has a BET surface area of 594 m^2/g, a pore volume of 0.69 cm^3/g, and a narrow pore size distribution centered at 36.8 Å. Furthermore, the structure and morphology of the SBA-16 were analyzed by SEM (Fig. 1C), and it reveals many decaoctaheron-shape domains that aggregate into microstructures with relatively uniform size (2–6 μm), which is in good agreement with the previous reports [24].

Textural characteristics of catalysts

The N_2-physisorption isotherms and pore size distributions for the catalysts are shown in Fig. 2. The Au–Pd/SBA-16 catalyst exhibits a typical type-IV isotherm with a pronounced hysteresis loop characteristic of cage-like materials with interconnected uniform mesopores [26]. For the Au–Pd/SBA-16-CeO_2 catalyst, although the isotherm shows a slight difference as compared with SBA-16, it still indicates that the mesostructure is maintained. The change in the shape of the hysteresis loop is probably due to the obstruction of the pores by the CeO_2 particles. Similar phenomenon has been observed in TiO_2/SBA-16 catalyst [27]. The specific surface areas and pore volumes of the samples are summarized in Table 1. Compared to the corresponding supports, the BET surface areas and pore volumes of Au–Pd/SBA-16 and Au–Pd/SBA-16-CeO_2 catalysts are smaller, which suggests that the metal particles are not only dispersed on the surface of supports but also inside the pores [28]. Interestingly, in spite of the obvious decrease in the pore volumes and BET surface areas of the two catalysts, their pore diameters do not show significant changes. This probably means that the pores are only partly blocked by the metal species, as described previously by Tsoncheva et al. [29]. For CeO_2 support, after loading Au–Pd, the BET surface area increases, which is similar to the work reported by Hiroaki et al. [30].

XRD of catalysts

Figure 3 illustrates the XRD patterns of Au–Pd/SBA-16, Au–Pd/SBA-16-CeO_2, and Au–Pd/CeO_2 catalysts calcined at 400 °C. In Fig. 3A, the two patterns are similar and show the (110) reflection (0.92°) of the cubic mesopore structure, which is in accordance with the N_2-physisorption analysis. Figure 3B depicts the wide-angle XRD patterns of the three catalysts. Peaks of 28.5°, 32.8°, 47.5°, and 57.5°, which are observed in Au–Pd/SBA-16-CeO_2 and Au–Pd/CeO_2 catalysts, are assigned to the diffraction patterns of CeO_2 (111),

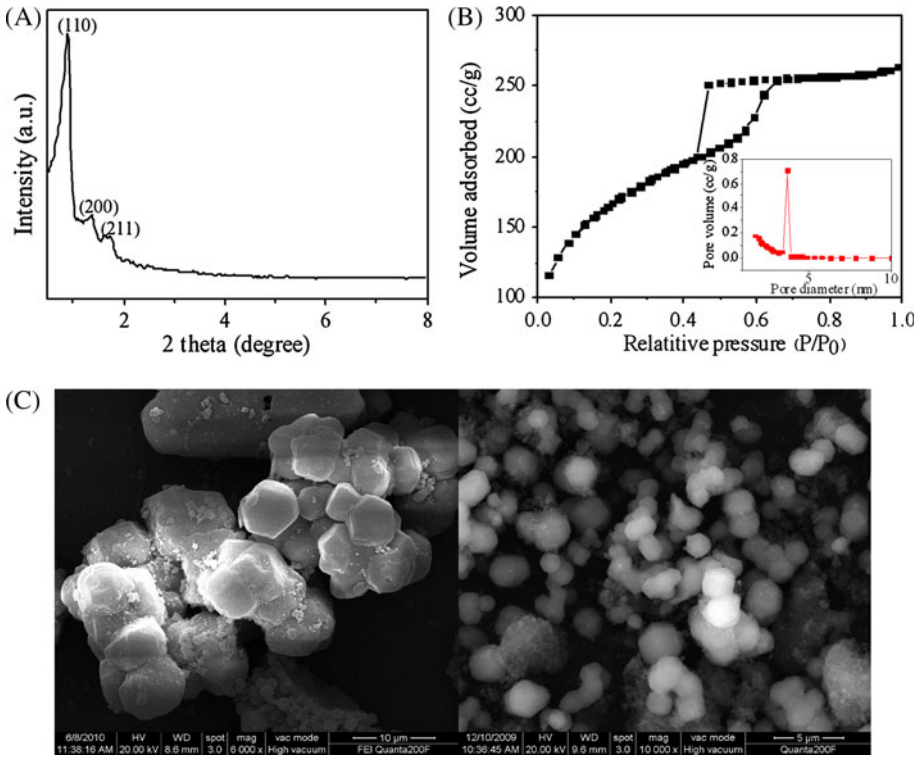

Fig. 1 Small-angle XRD pattern (**A**), N_2 adsorption–desorption isotherm (**B**), and SEM images of calcined SBA-16 support

Table 1 Textural properties of the supports and catalysts

Samples	S_{BET} (m^2/g)	Pore volume (cm^3/g)	Average pore diameter (Å)
SBA-16	594	0.69	36.8
SBA-16-CeO_2	476	0.57	37.5
CeO_2	82	0.16	75.9
Au–Pd/SBA-16	410	0.42	36.7
Au–Pd/SBA-16-CeO_2	306	0.48	35.9
Au–Pd/CeO_2	92	0.18	75.5

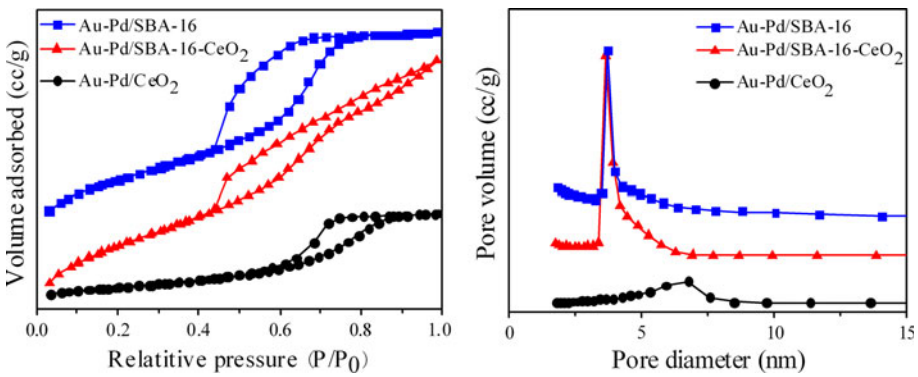

Fig. 2 N_2-physisorption isotherms and pore size distributions of catalysts

(200), (220), and (311) planes, respectively [21]. A broad peak at 22.6° corresponds to the amorphous SiO_2 reflection in Au–Pd/SBA-16 and Au–Pd/SBA-16-CeO_2 catalysts [27]. It is interesting to note that the diffraction peaks at 38.9° and 44.8° attributed to the Au_xPd_y alloys are observed in Au–Pd/SBA-16 and Au–Pd/SBA-16-CeO_2 catalysts [12]. Furthermore, the peak intensities of Au_xPd_y alloys in Au–Pd/SBA-16 catalyst are higher than those in Au–Pd/SBA-16-CeO_2 catalyst. These results reveal that the SBA-16 promotes the formation of Au_xPd_y alloys while the CeO_2 prohibits the process. Venezia et al. [31, 32] considered that gold had a trend to capture palladium into its lattice,

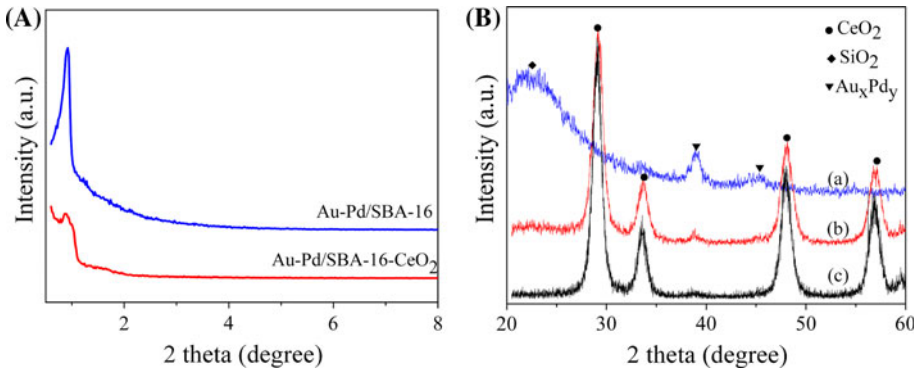

Fig. 3 Small-angle XRD patterns of Au–Pd/SBA-16 and Au–Pd/SBA-16-CeO_2 (**A**); wide-angle XRD patterns of the catalysts: *a* Au–Pd/SBA-16, *b* Au–Pd/SBA-16-CeO_2, *c* Au–Pd/CeO_2 (**B**)

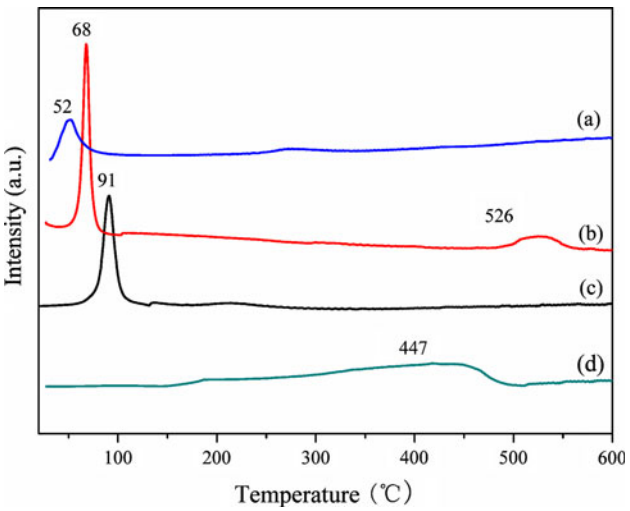

Fig. 4 TPR profiles of the samples: *a* Au–Pd/SBA-16, *b* Au–Pd/SBA-16-CeO_2, *c* Au–Pd/CeO_2, *d* CeO_2

forming Au_xPd_y alloys, which facilitated the improvement of catalytic performance.

TPR studies of catalysts

The TPR profiles of the pure CeO_2, Au–Pd/SBA-16, Au–Pd/SBA-16-CeO_2, and Au–Pd/CeO_2 catalysts are depicted in Fig. 4. The low-temperature reduction peaks at ca. 52, 68 and, 91 °C are observed in Au–Pd/SBA-16, Au–Pd/SBA-16-CeO_2, and Au–Pd/CeO_2 catalysts, respectively, which may be attributed to the reduction of Au_xO_y, PdO, Au_xPd_yO and even part of superficial CeO_2. The increase in the reduction temperature is probably due to the increase in the interactions between the Au, Pd particles and supports. Further inspection of these TPR profiles also reveals that both Au–Pd/SBA-16-CeO_2 and Au–Pd/CeO_2 catalysts exhibit higher H_2 consumption than Au–Pd/SBA-16 catalyst, implying the reduction of superficial CeO_2. It is noteworthy that the reduction temperatures of superficial CeO_2 in Au–Pd/SBA-16-CeO_2 (68 °C) and Au–Pd/CeO_2 (91 °C) catalysts are much lower than the pure superficial CeO_2 (447 °C), which could be owing to the metal-CeO_2 interactions and the H_2 spillover from metals to CeO_2. Noticeably, another reduction peak at 526 °C is observed in Au–Pd/SBA-16-CeO_2 catalyst, indicating the reduction of the bulk-phase lattice oxygen of CeO_2. The reduction temperature of bulk CeO_2 in Au–Pd/SBA-16-CeO_2 catalyst is much lower than the temperature (over 750 °C) reported by Yao et al. [33], which could also be attributed to the H_2 spillover. The comparison of Au–Pd/SBA-16-CeO_2 and Au–Pd/CeO_2 catalysts demonstrates that the bulk CeO_2 reduction peak does not appear in the Au–Pd/CeO_2 catalyst, suggesting that the SBA-16 promotes the dispersion of CeO_2, which favors the reduction of the bulk CeO_2.

H_2-TPD profiles of the catalysts

Figure 5 presents the H_2-TPD profiles of the Au–Pd/SBA-16, Au–Pd/SBA-16-CeO_2, and Au–Pd/CeO_2 catalysts. The comparison of the three TPD profiles indicates that the H_2 desorption temperatures increase in the following order: Au–Pd/SBA-16 catalyst < Au–Pd/SBA-16-CeO_2 catalyst < Au–Pd/CeO_2 catalyst, probably owing to the existence of metal-CeO_2 interactions. The lower desorption temperature makes desorption of reaction product H_2 easier, which is beneficial to the POM reaction. On the basis of XRD as well as TPR and TPD results, we proposed that metal-CeO_2 interactions can impede the formation of Au_xPd_y alloys, and the Au_xPd_y alloys exhibit lower H_2 desorption temperature.

Catalytic activity

CH_3OH conversion, O_2 conversion, H_2 selectivity, and CO selectivity for POM reaction were studied on Au–Pd/SBA-16, Au–Pd/SBA-16-CeO_2, and Au–Pd/CeO_2 catalysts from 200 to 450 °C (Figs. 6, 7). As shown in Fig. 6, Au–Pd/SBA-16 and Au–Pd/SBA-16-CeO_2 catalysts exhibit higher CH_3OH conversion and H_2 selectivity when compared to Au–Pd/CeO_2 catalyst, probably due to the formation of Au_xPd_y alloys and their larger BET surface areas. It is

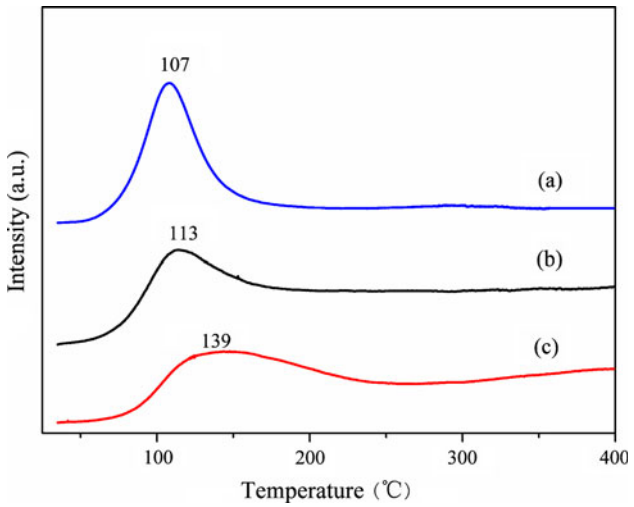

Fig. 5 H_2-TPD profiles of the catalysts: *a* Au–Pd/SBA-16, *b* Au–Pd/SBA-16-CeO_2, *c* Au–Pd/CeO_2

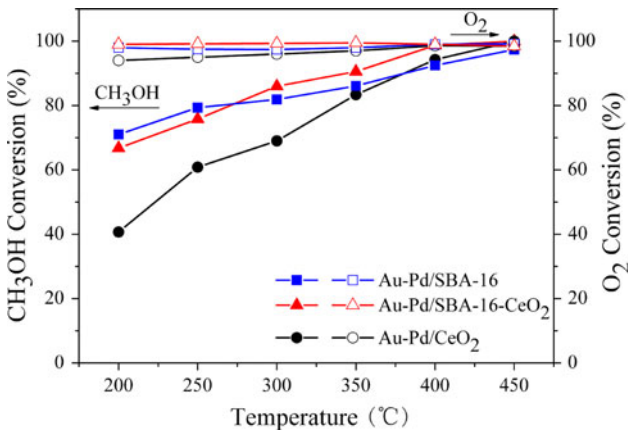

Fig. 6 Effect of reaction temperature on CH_3OH conversion and O_2 conversion over the catalysts for POM reaction

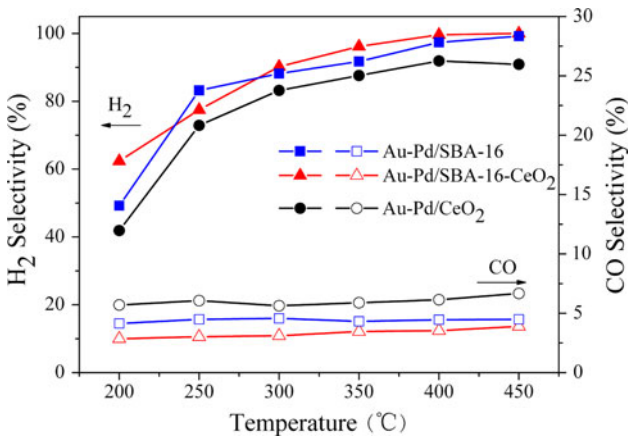

Fig. 7 Effect of reaction temperature on H_2 selectivity and CO selectivity over the catalysts for POM reaction

noteworthy that the BET surface area of Au–Pd/SBA-16-CeO_2 catalyst is lower than that of Au–Pd/SBA-16 catalyst, but the two catalysts show similar catalytic activity. This demonstrates that the Au_xPd_y alloys play a more important role in the POM reaction than BET surface area. In all catalytic systems, oxygen is completely consumed throughout the examined temperature range. CH_3OH conversion and H_2 selectivity increase with increasing reaction temperatures. This could be explained here.

Initially, CH_3OH quickly consumes O_2 leading to highly exothermic methanol combustion (MC) reaction (Eq. (1)) with production of H_2O and CO_2 [34]. Since O_2 has been completely consumed, the other CH_3OH consumption reactions have taken place during POM reaction (Eq. (2)).

$$CH_3OH + 1.5O_2 \rightarrow 2H_2O + CO_2 \quad (1)$$

$$CH_3OH + 0.5O_2 \rightarrow 2H_2 + CO_2 \quad (2)$$

When the temperature increases from 250 to 300 °C, the H_2O formed via MC reaction may be consumed by SRM reaction (Eq. (3)), leading to the increase in H_2 selectivity with consequent decrease in H_2O selectivity [35].

$$CH_3OH + H_2O \rightarrow 3H_2 + CO_2 \quad (3)$$

With the further increasing of the reaction temperatures, no more O_2 is available and the MD reaction predominates, thus leading to more H_2 and CO formation (Eq. (4)).

$$CH_3OH \rightarrow 2H_2 + CO \quad (4)$$

CO produced by the side reactions is subsequently transformed into CO_2 by the WGS reaction (Eq. (5)) or CO oxidation (Eq. (6)).

$$CO + H_2O \rightarrow H_2 + CO_2 \quad (5)$$

$$CO + 0.5O_2 \rightarrow CO_2 \quad (6)$$

Formerly, supported Au–Pd catalyst has been reported to be an efficient catalyst for low-temperature CO oxidation [32], which explains the low amount of CO during POM reaction over the three catalysts. The comparison of CO selectivity for the three catalysts demonstrates that both Au–Pd/SBA-16 and Au–Pd/SBA-16-CeO_2 catalysts show lower CO selectivity than Au–Pd/CeO_2 catalyst, which indicates that the Au_xPd_y alloys can promote CO oxidation [32]. Further inspection of Au–Pd/SBA-16 and Au–Pd/SBA-16-CeO_2 catalysts reveals that CO selectivity of Au–Pd/SBA-16-CeO_2 catalyst is lower than that of Au–Pd/SBA-16 catalyst, owing to the good activity of CeO_2 to oxidize CO into CO_2. The above results suggest that both the Au_xPd_y alloys and CeO_2 can facilitate the oxidation of CO. As revealed by the Figs. 6, 7, the Au–Pd/SBA-16-CeO_2 exhibits 100% CH_3OH conversion, 99.2% H_2 selectivity, and 3.9% CO selectively at 450 °C.

Conclusion

Au–Pd/SBA-16, Au–Pd/SBA-16-CeO_2, and Au–Pd/CeO_2 catalysts were prepared by deposition–precipitation technique and examined by BET, XRD, TPR, and H_2-TPD analyses. The results show that the SBA-16 promotes the formation of Au_xPd_y alloys while the metal-CeO_2 interactions impede this process. The three catalysts were also studied for partial oxidation of methanol to produce H_2. Au–Pd/SBA-16 and Au–Pd/SBA-16-CeO_2 catalysts showed higher activity and selectivity than Au–Pd/CeO_2 catalyst. Compared with Au–Pd/SBA-16 catalyst, Au–Pd/SBA-16-CeO_2 catalyst showed the lower CO selectivity. The results reveal that the Au_xPd_y alloys play an important role in the POM reaction. Both the Au_xPd_y alloys and CeO_2 facilitate the oxidation of CO.

Acknowledgments This work was supported by the National Natural Science Foundations of China (20701018 and 21062013) and the Foundation of Educational Department of Jiangxi Province (GJJ08024).

References

1. Appleby AJ, Foulkes FR (1989) Fuel cell hand book. Van Nostrand Reinhold, NewYork
2. Granovskii M, Dincer I, Rosen MA (2006) Int J Hydrogen Energy 31:337
3. Cheng WH (1995) Appl Catal A Gen 130:13
4. Yong ST, Hidajat K, Kawi S (2008) Catal Today 131:188
5. Matter PH, Ozkan US (2005) J Catal 234:463
6. Lin SSY, Thomson WJ, Hagensen TJ, Ha SY (2007) Appl Catal A Gen 318:121
7. Kulprathipanja A, Falconer JL (2004) Appl Catal A Gen 261:77
8. Cubeiro ML, Fierro JLG (1998) J Catal 179:150
9. Turco M, Bagnasco G, Costantino U, Marmottini F, Montanari T, Ramis G, Busca G (2004) J Catal 228:56
10. Turco M, Bagnasco G, Cammarano C, Senese P, Costantino U, Sisani M (2007) Appl Catal B 77:46
11. Cubeiro ML, Fierro JLG (1998) Appl Catal A Gen 168:307
12. Wang JX, Luo LT (2008) Catal Lett 126:325
13. Schuyten S, Guerrero S, Miller JT, Shibata T, Wolf EE (2009) Appl Catal A Gen 352:133
14. Eswaramoorthi I, Dalai AK (2009) Int J Hydrogen Energy 34:2580
15. Haruta M, Yamada N, Kobayashi T, Iijima S (1989) J Catal 115:301
16. Haruta M, Tsubota S, Kobayashi T, Kageyama H, Genet MJ, Delmon B (1993) J Catal 144:175
17. Sakamoto Y, Kaneda M, Terasaki O, Zhao DY, Kim JM, Stucky GD, Shim HJ, Ryoo R (2000) Nature 408:449
18. Mesa M, Sierra L, Patarin J, Guth JL (2005) Solid State Sci 7:990
19. Yu CZ, Fan J, Tian BZ, Zhao DY (2004) Chem. Mater 16:889
20. Yu CZ, Tian BZ, Fan J, Stucky GD, Zhao DY (2002) J Am Chem Soc 124:4556
21. Chen QB, Luo LT (2008) Indian J Chem Sect A 47:1317
22. Andreeva D, Idakiev V, Tabakova T, Ilieva L, Falaras P, Bourlinos A, Travlos A (2002) Catal Today 72:51
23. Fu Q, Deng WL, Saltsburg H, Stephanopoulos MF (2005) Appl Catal B 56:57
24. Jin HX, Wu QY, Chen C, Zhang DL, Pang WQ (2006) Microporous Mesoporous Mater 97:141
25. Kleitz F, Solovyov LA, Anikumar GA, Choi SH, Ryoo R (2004) Chem Commun 13:1536
26. Huo QS, Leon R, Petroff PM, Stucky GD (1995) Science 268: 1324
27. Ma J, Qiang LS, Tang XB, Li HY (2010) Catal Lett 138:88
28. Hess C, Hoefelmeyer JD, Tilley TD (2004) J Phys Chem B 108: 9703
29. Tsoncheva T, Linden M, Areva S, Minchev C (2006) Catal Commun 7:357
30. Sakurai H, Tsubota S, Haruta M (1993) Appl Catal A Gen 102: 125
31. Venezia AM, Parola VL, Deganello G (2002) J Catal 212:56
32. Venezia AM, Liotta LF, Pantaleo G (2003) Appl Catal A Gen 251:359
33. Yao HC, Yao YFY (1984) J Catal 86:254
34. Chang FW, Roselin LS, Ou TC (2008) Appl Catal A Gen 334:147
35. Agrell J, Birgersson H, Boutonnet M, Cabrera IM, Navarro RM, Fierro JLG (2003) J Catal 219:389